The deposition of particulates in turbulent pipe flow
by Charles Kenneth Sande

A thesis submitted in partial fulfillment of the requirements for the degree of MASTER OF SCIENCE in Mechanical Engineering
Montana State University
© Copyright by Charles Kenneth Sande (1976)

Abstract:
A model was developed for the deposition of particulates for turbulent flow in a circular tube and the deposition rate of the particles on the wall of the tube was predicted. The tube configurations considered (diameter x length) were 19 mm x 3.66 m, 19 mm x 6.1 m, 38 mm x 7.6 m, and 51 mm x 12.2 m. The flow parameters (fluid temperatures and velocities) were those expected for the cored brick, regenerative heat exchangers proposed for preheating the combustion air in open cycle magnetohydrodynamic (MHD) cycles.

A theoretical model was developed based on mass transport within the tube resulting from turbulent radial diffusion and bulk mass convection due to the mean velocity field in the axial direction. Expressions developed from the Navier-Stokes equations were coupled with empirical data on turbulent flow to describe the turbulent diffusion process. A development based on Stoke's law and the energy density spectrum of the fluid turbulence was used to approximate the turbulent diffusion coefficient of the particles. The resulting finite difference equations were solved using a digital computer.

For the seven test cases studied, particles less than 10 μm in diameter have approximately equal response characteristics to turbulent eddies and deposit at very high rates. The deposition rate drops sharply as the particle diameter exceeds 20 ym. Both increased wall roughness and increased flow velocity enhance particle deposition rates significantly. Because of their higher volume to surface area ratios, large diameter tubes experience lower deposition rates at the entrance but higher deposition rates at axial positions further along the tube than do small diameter tubes.

STATEMENT OF PERMISSION TO COPY

In presenting this thesis in partial fulfillment of the requirements for an advanced degree at Montana State University, I agree that the Library shall make it freely available for inspection. I further agree that permission for extensive copying of this thesis for scholarly purposes may be granted by my major professor, or, in his absence, by the Director of Libraries. It is understood that any copying or publication of this thesis for financial gain shall not be allowed without my written permission.

Signature C. Kenneth Sorde

Date 20 October 1976

THE DEPOSITION OF PARTICULATES IN TURBULENT PIPE FLOW

by

CHARLES KENNETH SANDE

A thesis submitted in partial fulfillment
of the requirements for the degree

of

MASTER OF SCIENCE

in

Mechanical Engineering

Approved:

Harry W. Downs
Chairperson, Graduate Committee

Dennis O. Blackketter
Head, Major Department

Henry L Parsons
Graduate Dean

MONTANA STATE UNIVERSITY
Bozeman, Montana

October, 1976

Acknowledgments

The author acknowledges Dr. H.W. Townes and Dr. T.C. Reihman for their assistance in preparing this thesis. A special thanks goes to the author's parents, for their many years of training, guidance, and support.

TABLE OF CONTENTS

Chapter		Page
	Vita	ii
	Acknowledgments	iii
	List of Tables	v
	List of Figures	vi
	Nomenclature	vii
	Abstract	x
I.	Introduction	1
II.	Literature Review	2
III.	Theory	3
IV.	Results	16
V.	Conclusions	23
VI.	Recommendations	24
	Tables	25
	Figures	29
	Appendix I	37
	Appendix II	44
	Appendix III	50
	Appendix IV	58
	Literature Cited	61

LIST OF TABLES

Table		Page
1	Test Case Particle Size Distribution	26
2	Test Case Flow Conditions	27
3	Test Case Flow Conditions	28

LIST OF FIGURES

Figure		Page
1	Energy Density Spectrum	30
2	Rate of Diameter Decrease for 19 mm x 3.66 m Tube	31
3	Rate of Diameter Decrease for 19 mm x 6.1 m Tube	32
4	Rate of Diameter Decrease for 19 mm x 6.1 m Tube and 51 mm x 12.2 m Tube	33
5	Exit Concentration Profiles for 19 mm Tube	34
6	Particle Size Distribution for 19 mm Tube	35

NOMENCLATURE

Symbol	Description
A	Cross-sectional area of tube
C	Mass concentration, mass of particles per unit mass of fluid
$c_{i,j}$	Mass concentration for numerical formulation at i^{th} radial increment and j^{th} axial increment
$\bar{c}_j$	Mean mass concentration at j^{th} axial increment
c_v	Volume concentration, mass of particles per unit volume
d	Particle diameter
D	Total (molecular plus turbulent) diffusion coefficient for particles
D_m	Molecular diffusion coefficient for particles
D_p	Pipe diameter
f_i	Interaction coefficient relating eddy diffusivity of momentum to particle eddy diffusivity of mass
f_k	Weighting factor equal to fraction of total turbulent energy contained in the k^{th} frequency band of the energy density spectrum
f_x	Friction factor
F	Slip factor for molecular diffusion coefficient
F_D	Viscous drag force imparted to a particle suspended within a turbulent fluid

Symbol	Description
k	Boltzman's constant
K	Tube wall roughness
$\ln$	Logarithm to base e
m_p	Particle mass
$\dot{m}_D$	Mass flux rate of particles to wall of tube
$\dot{M}_j$	Axial mass flux of particles at j^{th} axial increment
$\Delta m_{i,j}$	Mass contained in i^{th} annular volume at j^{th} axial increment
r	Radial position measured from tube center
R	Tube radius
Re	Reynolds Number = VD_p/ν
$\dot{R}$	Rate of decrease of pipe radius
Δr_i	Radial increment = $r_i - r_{i-1}$
T_k	Absolute temperature
u	Mean axial fluid velocity
u_*	Shear velocity = $(\tau_o/\rho_f)^{1/2}$
$\overline{u'v'}$	Time average of axial and radial fluctuating velocity components
v	Mean radial fluid velocity
v_f	Fluid radial fluctuating velocity for interaction coefficient
v_p	Particle radial fluctuating velocity for interaction coefficient
v_{po}	Initial particle radial fluctuating velocity

Symbol	Description
V	Mean bulk axial fluid velocity
$\forall$	Volume
w	Mean angular fluid velocity
x_f	Fluid displacement from its mean position
x_p	Particle displacement from its mean position
x_{pm}	Maximum particle displacement from its mean position
x_{po}	Initial particle displacement from its mean position
X_o	Maximum fluid displacement from its mean position
y	Radial position measured from wall
z	Axial position
Δz	Axial increment
ε_f	Fluid eddy diffusivity of momentum
ε_p	Particle eddy diffusivity of mass
ρ_f	Fluid density
ρ_p	Particle density
μ	Fluid dynamic viscosity
ν	Fluid kinematic viscosity
τ_o	Wall shear stress
ϕ	Angular position
ω	Circular frequency of fluid turbulence

Abstract

A model was developed for the deposition of particulates for turbulent flow in a circular tube and the deposition rate of the particles on the wall of the tube was predicted. The tube configurations considered (diameter x length) were 19 mm x 3.66 m, 19 mm x 6.1 m, 38 mm x 7.6 m, and 51 mm x 12.2 m. The flow parameters (fluid temperatures and velocities) were those expected for the cored brick, regenerative heat exchangers proposed for preheating the combustion air in open cycle magnetohydrodynamic (MHD) cycles.

A theoretical model was developed based on mass transport within the tube resulting from turbulent radial diffusion and bulk mass convection due to the mean velocity field in the axial direction. Expressions developed from the Navier-Stokes equations were coupled with empirical data on turbulent flow to describe the turbulent diffusion process. A development based on Stoke's law and the energy density spectrum of the fluid turbulence was used to approximate the turbulent diffusion coefficient of the particles. The resulting finite difference equations were solved using a digital computer.

For the seven test cases studied, particles less than 10 μm in diameter have approximately equal response characteristics to turbulent eddies and deposit at very high rates. The deposition rate drops sharply as the particle diameter exceeds 20 μm. Both increased wall roughness and increased flow velocity enhance particle deposition rates significantly. Because of their higher volume to surface area ratios, large diameter tubes experience lower deposition rates at the entrance but higher deposition rates at axial positions further along the tube than do small diameter tubes.

I. Introduction

Proposed open cycle magnetohydrodynamic (MHD) cycles require gas temperatures in the MHD channel of approximately 3000 K. Since this temperature cannot be achieved by the combustion of coal and relatively low temperature air, it is necessary to preheat the combustion air. One method for preheating the air is by means of cored ceramic brick regenerative heat exchangers. Since the heat source for these heat exchangers is the combustion products from the MHD channel, it is necessary to determine what effect the coal combustion products and seed material will have on the heat exchanger performance. One anticipated effect is the deposition of coal slag and seed material on the walls of the flow passages of the cored brick. This will be a major factor effecting the performance of the heat exchanger. The determination of the particulate deposition rate is therefore of primary importance in the design and operation of the air preheaters. The objective of this work is to provide a means to model the flow system mathematically and predict the particulate deposition characteristics.

II. Literature Review

The diffusion and deposition of particles from turbulent flow streams has been studied both analytically and experimentally. Schlinger and Sage [1], and Longwell and Weiss [2] investigated the mixing and diffusion of liquids in turbulent gas streams and present correlations between theoretically predicted results and those obtained experimentally. Davies [3] presents a theoretical model of the deposition of particles from a moving aerosol, and Friedlander and Johnstone [4] provide both experimental and analytic information on the deposition of suspended particles from turbulent gas streams. The analytic work done by Davies and by Friedlander and Johnstone provides a starting point for the model developed in this thesis.

An analytic development describing the diffusion and deposition of particles from a turbulent flow stream must contain complete information on both the flow stream characteristics and the behavior of the particles suspended within the flow. A description of the mean flow characteristics of turbulent flow was obtained from Powe, Townes, and Gow [5]. Studies by Powe [6], Schlichting [7], and Laufer [8] were used to describe the eddy characteristics of turbulent flow. Information on molecular diffusion coefficients of particles was obtained from Einstein [9] and Davies [3]. Longwell and Weiss [2] and Hinze [10] provide information leading to a correlation between the eddy diffusion of fluid momentum and the eddy diffusion of mass for suspended particles.

III. Theory

Current designs for MHD regenerative cored brick heat exchangers are based on a hexagonal array of flow passages with circular cross-sections. The model which is developed describes the axial flow of air and the transport of suspended particles both axially and radially within a circular tube.

The following equation can be developed by application of the conservation of mass principle to a cylindrical control volume. [12]

$$\left[\frac{\partial}{\partial r}\left(rD\,\frac{\partial c_v}{\partial r}\right)+\frac{\partial}{\partial z}\left(rD\,\frac{\partial c_v}{\partial z}\right)+\frac{\partial}{\partial \phi}\left(\frac{D}{r}\,\frac{\partial c_v}{\partial \phi}\right)\right]$$

$$-\left[\frac{\partial}{\partial r}\left(c_v v r\right)+\frac{\partial}{\partial z}\left(c_v u r\right)+\frac{\partial}{\partial \phi}\left(c_v w r\right)\right]=r\,\frac{\partial c_v}{\partial t} \qquad (1)$$

where D = total (turbulent plus molecular) diffusion coefficient for the particles
c_v = mass of particles per unit volume of fluid
r = radial position
z = axial position
ϕ = angular position
v = mean radial velocity
u = mean axial velocity
w = mean angular velocity

The terms in the first set of brackets describe the molecular and turbulent diffusion of mass due to a concentration gradient, and the terms in the second set of brackets describe the bulk transfer

of mass due to the mean fluid velocity in the three coordinate directions.

For steady flow conditions, with axial symmetry, and for the radial mass transport due entirely to diffusion and the axial transport due entirely to bulk transfer, equation (1) may be expressed in differential form as

$$\frac{D}{u}\frac{\partial^2 c}{\partial r^2} + \frac{1}{ru}\frac{\partial c}{\partial r}\left(D + r\frac{\partial D}{\partial r}\right) - \frac{\partial c}{\partial z} = 0 \qquad (2)$$

where the substitution $c_v = c\rho_f$ has been made in which

c = mass of particles per unit mass of fluid, and

ρ_f = density of the fluid.

Equation (2) is a non-linear partial differential equation, since D is a non-linear function of both r and z. A numerical solution is therefore required. The finite difference form of equation (2) with the i and j subscripts indicating radial and axial locations, respectively, is

$$c_{i,j+1} = c_{i+1,j}(\alpha_1 + \alpha_2) + c_{i,j}(1 - \alpha_1 - \alpha_2) + c_{i-1,j}(\alpha_4) \qquad (3)$$

$$\text{where } \alpha_1 = \frac{\Delta z}{ru\Delta r_{i+1}}\left(D + r\left.\frac{\partial D}{\partial r}\right|_i\right) \qquad (4)$$

$$\alpha_2 = \frac{2D\Delta z}{u\Delta r_{i+1}} \cdot \frac{1}{\Delta r_i + \Delta r_{i+1}} \qquad (5)$$

$$\alpha_3 = \frac{2D\Delta z}{u\Delta r_{i+1}\Delta r_i} \tag{6}$$

$$\alpha_4 = \frac{2D\Delta z}{u\Delta r_i} \cdot \frac{1}{\Delta r_i \Delta r_{i+1}} \tag{7}$$

where Δz is the size of the axial increment and $\Delta r_i = r_i - r_{i-1}$.

The boundary condition at the center of the tube is that the radial mass flux be equal to zero, or

$$\frac{\partial c}{\partial r} = 0 \quad \text{at} \quad r = 0. \tag{8}$$

The boundary condition at the wall is based on the assumption that every particle striking the wall permanently adheres to the wall. The particles are assumed to strike the wall when their centers are at a distance of one particle radius from the outermost surface of the wall. This indicates a layer of zero particle concentration at a distance from the wall equal to the sum of one particle radius plus the wall roughness, i.e.

$$c = 0 \quad \text{at} \quad y = \frac{d}{2} + K \tag{9}$$

where y is the distance from the tube wall, d is the particle diameter, and K is the wall roughness.

Although the equations are valid for a zero wall roughness and the numerical procedure converges, the axial steps required to maintain equation stability are extremely small, thus producing very long run times for the numerical solution. Because of this fact, and since zero

wall roughness is an unrealistic situation, no results are presented for the case of zero wall roughness.

The boundary condition assuming that the particles permanently adhere to the wall is not always valid. Some particles may become re-entrained in the fluid, or for high temperature flows and for the case of a verticle tube, the particles may still be in a liquid state and flow down the tube wall. However, such behavior is not considered in this analysis.

The initial condition for the solution of equation (3) may be formed to suit a variety of flow situations. For this analysis, a perfectly flat concentration profile was taken at the entrance of the tube. [For further details on the development of the equation for turbulent diffusion and bulk transfer of particles, see Appendix I].

Diffusion of particles suspended in a fluid results from either molecular or turbulent transport of mass due to a concentration gradient. The calculation of the molecular diffusion coefficient, D_m, is based upon kinetic theory. Turbulent diffusion is caused by the particles' interaction with the turbulent fluid and is represented by ε_p, the particles' eddy diffusivity of mass. If the fluid motion is characterized by ε_f, the eddy diffusivity of momentum, the interaction between the particles and the fluid can be represented by a postulated interaction coefficient, f_i, defined in the relation

$$\varepsilon_p = \varepsilon_f \cdot f_i \tag{10}$$

For turbulent flow, the molecular diffusion of particles is much smaller than the eddy diffusion of particles, and the total diffusion coefficient may be approximated as

$$D = D_m + \varepsilon_p \doteq \varepsilon_p = \varepsilon_f \cdot f_i \qquad (11)$$

An expression for ε_f based on local velocities can be obtained from the time-average Navier-Stokes equations as shown by Schlichting [7]. The resulting expression is

$$\varepsilon_f = \overline{u'v'}/d\bar{u}/dy \qquad (12)$$

where $\overline{u'v'}$ is the time average of the axial and radial fluctuating velocity components and $d\bar{u}/dy$ is the mean velocity gradient.

Laufer [8] related $\overline{u'v'}$ to the mean velocity field, showing that

$$\overline{u'v'} = \nu \frac{d\bar{u}}{dr} + \frac{r}{R} u_*^2 \qquad (13)$$

This can be rewritten by making the coordinate transformation

$$r = R - y, \qquad dr = -dy \qquad (14)$$

as

$$\overline{u'v'} = -\nu \frac{d\bar{u}}{dy} + \frac{R-y}{R} u_*^2 \qquad (15)$$

where ν is the fluid kinematic viscosity, R is the tube radius, and u_* is the friction velocity which is given by

$$u_* = \left(\tau_o/\rho_f\right)^{1/2} \qquad (16)$$

The wall shear stress, τ_o, is defined in terms of the mean axial fluid velocity, V, as

$$\tau_o = \frac{f_x}{4} \cdot \frac{\rho_f V^2}{2g_c} \qquad (17)$$

where f_x is the friction factor. For Reynolds numbers less than 10^5, the Blasius expression for f_x [12] agrees well with experimental data. This relation is

$$f_x = 0.316/Re^{1/4} \qquad (18)$$

where

$$Re = VD_p/\nu \qquad (19)$$

Equations (16) and (17) may be combined to give

$$u_* = V\,(f_x/8)^{1/2} \qquad (20)$$

An expression for $d\bar{u}/dy$ may be obtained by using the two equation mean velocity profile given by Powe, Townes, and Gow [5] as

$$\bar{u} = u_* c_1 \mathrm{Tanh}(x/c_1) \qquad x \leq x_o \qquad (21)$$

and

$$\bar{u} = u_* (a_1 \ln(x) + b) \qquad x > x_o \qquad (22)$$

The constants a_1, b_1, c_1, and x_o are empirically determined with the values of 2.42, 5.98. 14.68, and 27.75, respectively, and were obtained for Reynolds numbers ranging from 6×10^4 to 3×10^5. The parameter x is defined as

$$x = 3yu_*(2-y/R)/(2\nu(3+4y/R + 2y^2/R^2)) \qquad (23)$$

For the flow conditions used in this study, there is little available information on the development of the velocity profile in the entrance region of the tube. Therefore, a fully developed velocity profile is assumed at the tube entrance. For similar flow systems, the actual entrance effects reduce mass diffusion so the results obtained in this analysis will be conservative, giving larger deposition rates than would be expected in the entrance region of actual flow systems.

Combining equations (12) and (15), and taking the derivatives of equations (21) and (22) to obtain $d\bar{u}/dy$, gives the expressions for ε_f as

$$\varepsilon_f = -\nu + \frac{\nu}{\operatorname{sech}^2(x/c_1)} \cdot \frac{(3-4y/R + 2y^2/R^2)}{9-9y/R} \qquad x \leq x_o \qquad (24)$$

and

$$\varepsilon_f = -\nu + \nu \cdot \frac{x}{a_1} \cdot \frac{(3-4y/R + 2y^2/R^2)}{9-9y/R} \qquad x < x_o \qquad (25)$$

Equations (24) and (25) are based on the velocity expressions derived for high Reynolds number flow systems, whereas, the Reynolds numbers for the flow in regenerative heat exchangers are expected to range only as high as about 4000. For the lower Reynolds number flows, the curve given by equations (24) and (25) reaches zero at an appreciable distance from the wall. Therefore, a slight modification to equations (24) and (25) is required to approximate the eddy diffusivity of momentum.

Because of the low Reynolds numbers used in this study, it is not known whether the flow system will behave as a rough wall or smooth wall system. This aspect of fluid mechanics is not well understood and no attempt is made to account for the effect of the rough walls on the expression for ε_f. [For further details on the development of the eddy diffusivity of momentum equation, see Appendix II.]

Although the effect of fluid turbulence on momentum transfer in the fluid may be characterized by the eddy diffusivity of momentum, a similar relationship for the effect of fluid turbulence on the diffusion of particles is not available. Therefore, a relationship between the diffusion of momentum and the diffusion of suspended particles in turbulent flow must be developed. It is reasonable to relate the particle diffusivity of mass, ε_p, to the fluid diffusivity of momentum, ε_f, through an interaction coefficient, f_i. If the velocity fluctuations in turbulent flow are represented by a Fourier transform, a spectrum of sinusoids of varying frequency can be used to approximate the fluid turbulence. By applying Stoke's law to the drag force on the particle, the simplified response of the particle at a single frequency

$$m_p \frac{d^2x_p}{dt^2} = 3\pi\mu d \left(X_o \omega \cos\omega t - \frac{dx_p}{dt}\right) \qquad (26)$$

where m_p is the particle mass, d is the particle diameter, x_p is the particle displacement from its mean position, and X_o is the maximum

amplitude of the turbulent fluid fluctuations.

A more detailed form of the equation is developed by Hinze [9], but because of the relatively large ratio between the densities of the particles and the fluid, it is not required in this analysis.

The solution to equation (26) is

$$x_p = \left(\frac{\beta}{\omega^2+\alpha^2} - \frac{v_{po}}{\alpha}\right)e^{-\alpha t} + x_{po} + \frac{v_{po}}{\alpha} + \beta\left(\frac{\alpha}{\omega}\sin\omega t + \cos\omega t\right) \qquad (27)$$

where $\alpha = 3\pi\mu d/m_p$

$\beta = \alpha\omega X_o$

and v_{po} and x_{po} are the particle's initial velocity and displacement, respectively.

By differentiating equation (27), the maximum amplitude of particle motion, x_{pm}, can be found. Dividing x_{pm} by X_o, the ratio of the particle motion to the fluid motion may be expressed as

$$\frac{x_{pm}}{X_o} = \left(\frac{\alpha^2}{\omega^2+\alpha^2}\right)^{1/2} \qquad (28)$$

The argument is now made that the eddy diffusion coefficient of a particle is proportional only to the amplitude ratio between the particle and the fluid, and that therefore the ratio $\varepsilon_p/\varepsilon_f$ may be expressed as

$$\varepsilon_p/\varepsilon_f = \left(\frac{\alpha^2}{\omega^2+\alpha^2}\right)^{1/2} \qquad (29)$$

Longwell and Weiss [2] use a similar derivation and obtain the same ratio for x_{pm}/X_o as given in equation (28). They state that since

the frequency of motion of the particle is the same as that of the fluid, its velocity will be reduced in proportion to its amplitude. Further-more, they theorize that the eddy diffusion coefficient is proportional to the product of velocity and amplitude, and therefore that the ratio of $\varepsilon_p / \varepsilon_f$ should be expressed as

$$\frac{\varepsilon_p}{\varepsilon_f} = \left(\frac{x_{pm}}{X_o}\right)^2 = \frac{\alpha^2}{\omega^2+\alpha^2} \tag{30}$$

Although some experimental data on the deposition of small diameter particles is available, [4], it is insufficient to verify which form of the $\varepsilon_p/\varepsilon_f$ ratio is best.

If the velocity fluctuations in turbulent flow are represented by a Fourier series of harmonic fluctuations, the interaction coefficient in either form is dependent upon the frequency spectrum of the turbulence. The effect of the frequency spectrum of the turbulent flow on the interaction coefficient is given by modified forms of equations (29) and (30).

$$\varepsilon_p = \varepsilon_f \cdot \sum_{k=1}^{11} \left(\frac{\alpha^2}{\omega_k^2+\alpha^2}\right)^{1/2} \cdot f_k = \varepsilon_f \cdot f_{i1} \tag{31}$$

and

$$\varepsilon_p = \varepsilon_f \cdot \sum_{k=1}^{11} \left(\frac{\alpha^2}{\omega_k^2+\alpha^2}\right) \cdot f_k = \varepsilon_f \cdot f_{i2} \tag{32}$$

The summation term in equations (31) and (32) is one possible method for weighting the effect of each frequency band within the frequency spectrum of the turbulence. For this analysis, the spectrum was arbitrarily divided into eleven frequency bands. The weighting factor f_k, is based on the fraction of the total turbulent energy contained within each of the eleven frequency bands.

Energy spectrum data for high Reynolds number flow is available from the work of Powe [6]. There is no known empirical data available for low Reynolds number flows, and consequently the data from Powe was utilized for this analysis. It may be reasonable to assume that although the level of turbulent energy may change with Re, the relative distribution of the energy with respect to eddy frequency remains essentially the same.

Powe's [6] original data gives turbulent energy as a function of both frequency and radial position. However, because turbulent energy is not a strong function of radius, and there is an uncertainty as to the applicability of high Reynolds number data to this study, and because of the increased computations that would be required otherwise, the radial dependence was removed by using the energy density spectrum averaged over all radii at a given frequency. The resulting curve is shown in Figure 1.

It should be observed that since the particle mass may be expressed as $m_p = \pi d^3 \rho_p / 6$, α may be written as

$$\alpha = 18\mu/\rho_p d^2 \qquad (33)$$

This indicates that form 1 of the interaction coefficient will be inversely proportional to the square of the particle diameter and form 2 will be inversely proportional to the fourth power of particle diameter. Therefore, the interaction coefficient will be much smaller for larger particles that for smaller particles. [For further details on the development of the interaction coefficient, see Appendix III.]

Equation (3) may be used to describe the concentration profiles of the particles along the full length of the tube. The average concentration of particles at a tube cross-section may be derived from the concentration profile and expressed in terms of a weighted sum as

$$\bar{c}_j = \frac{1}{R^2}\left[c_{o,j}\left(\frac{\Delta r_1}{2}\right)^2 + \sum_{i=1}^{N-1} c_{i,j}(\Delta r_i + \Delta r_{i+1})r_i\right] \qquad (34)$$

The mass flow of particles across any cross-section of the tube may be expressed as

$$\dot{M}_j = \bar{c}_j \cdot (u\rho_f)_j \pi R^2 \qquad (35)$$

The difference between the mass flow between two adjacent cross-sections divided by the surface area of the tube between the sections gives the net mass flux of particles to the wall as

$$\dot{m}_D = (\dot{M}_{j+1} - \dot{M}_j)/2\pi R\Delta z$$

$$= \left[\left(\bar{c}_{j+1}(u\rho_f)_{j+1}\pi R^2\right) - \left(\bar{c}_j(u\rho_f)_j \pi R^2\right)\right]/2\pi R\Delta z. \qquad (36)$$

Or, since $u\rho_f$ is constant along the tube,

$$\dot{m}_D = (\bar{c}_{j+1} - \bar{c}_j)(u\rho_f)_{inlet} \cdot R/2\Delta z \qquad (37)$$

An alternate expression for the deposition rate is obtained by dividing $\dot{m}_D$ by the particle density, ρ_p,

$$\dot{R} = \dot{m}_D/\rho_\rho \qquad (38)$$

which gives the rate of change in the tube radius.

The assumption that $u\rho_f$ is constant is dependent upon the condition of a constant tube cross-sectional area. This analysis considers the flow system before the deposited layer of particles grows to a significant thickness. [For further details on the rate of deposition derivation, see Appendix IV].

IV. Results

Using the model developed for the deposition of particles on the tube wall, seven test cases were studied. A digital computer was used to do all computations. The flow conditions were based on configurations which would satisfy ECAS Base Case 1 [13] designs for regenerative heat exchangers. Three of the tube configurations investigated have the tube diameter by tube length dimensions of 19 mm x 6.1 m, 38.1 mm x 7.62 m, and 50.8 mm x 12.2 m. In addition, the 19 mm x 3.66 m tube which represents the slag deposition test facility constructed at Montana State University was also studied.

A variation in tube wall roughness was studied for both 19 mm tubes, and the two different interaction coefficients were considered for the 19 mm x 3.66 m tube. The flow systems modeled in each of the seven cases are specified in Tables 1 and 2.

The particle size distribution used in the studies is given in Table 1, and was obtained from the analysis of the ash resulting from the combustion of lignite coal from the Rosebud seam at Colstrip, Montana. It indicates the relative distribution of particulate diameters resulting from the combustion of coal and air in the Corette power plant in Billings, Montana. This distribution may change for MHD systems, but the model will accommodate any particle size distribution. The average density of coal slag, 2980 Kg/m^2 was also obtained from an analysis of

the same coal ash, and is the density of the individual solid particles, not of a conglomeration of particles.

The form of the concentration profile equation, equation (3), indicates a linear relationship between the total inlet weight concentration of particles and the deposition rate of particles along the tube wall. Although all test cases were run for a one percent inlet concentration, the results may be extended to any desired inlet concentration by the use of this linear relationship.

Particles suspended in a turbulent fluid are known to have a damping effect on the fluid turbulence, so the linear relationship cited above is reasonably valid only for relatively small particle concentrations.

The deposition rate versus axial position for each of the seven test cases is shown in Figures 2, 3, and 4. The three curves shown in Figure 2 indicate the deposition rates obtained for the 19 mm x 3.66 m tube. The three cases are: (1) 127 μm wall roughness, (2) 253 μm wall roughness, and (3) 253 μm wall roughness combined with the increased interaction coefficient given by equation (31). The latter case produces the highest deposition rates, and the 127 μm wall roughness case produces the lowest.

The deposition rate for the 127 μm wall roughness case decreases rapidly within the first thirty pipe diameters of the tube, and thereafter decreases at a much slower rate, in an almost linear fashion. Half of the total slag deposited in the tube is deposited within the

first sixty pipe diameters of the tube. The dual effect of rapidly decreasing particle concentration and a decline in the fluid turbulence as a result of a negative axial temperature gradient produces the expected decline in deposition along the tube axis.

Since the particles are assumed to hit the tube wall when their surfaces contact the most extended points of the wall, the increased deposition rate shown for a wall roughness of 253 μm is expected. Although the decline in the deposition rate within the first thirty pipe diameters is not so great as for the 127 μm case, the higher deposition rates all along the tube result in half of the slag deposited to be contained within the first fifty pipe diameters of the tube. Because of the much higher deposition rates, a larger percentage of the particles have been deposited within the tube than for the 127 μm case, as shown in Figure 6. Lower particle concentrations near the tube exit tend to offset the effect of the larger wall roughness, and the combination of these conflicting factors produces a deposition rate near the tube exit only eight percent greater than that determined for the 127 μm case.

As noted in equations (31) and (32), two forms of the interaction coefficient were to be considered in this analysis. Equation (31) gives form 1 of the $\varepsilon_p/\varepsilon_f$ ratio, and will produce the largest values for f_i, since x_{pm}/X_o is less than one for all cases, and equation (32), which gives form 2 of the $\varepsilon_p/\varepsilon_f$ ratio, uses the squared value of the x_{pm}/X_o ratio.

For form 2 of $\varepsilon_p/\varepsilon_f$, f_i varies from .969 for a 2 μm particle to .0013 for a 128 μm particle. For form 1 of $\varepsilon_p/\varepsilon_f$, the same particle sizes have interaction coefficients of .996 and .0253, respectively. As is expected, the squaring of the x_{pm}/X_o ratio has the most significant effect on the larger particles, decreasing f_i by as much as a factor of twenty, while changing the interaction coefficient for smaller particles by as little as three percent. Therefore, form 1 of $\varepsilon_p/\varepsilon_f$ results in a significantly larger deposition rate for larger particles, as shown in Figure 6.

For example, for the 253 μm wall roughness case, and for form 2 of $\varepsilon_p/\varepsilon_f$, sixty-five percent of the 1.59 μm particles, and six percent of the 128 μm particles entering the tube have been deposited on the wall. However, for the same wall roughness but for form 1 of $\varepsilon_p/\varepsilon_f$ eighty-five percent of the 1.59 μm particles and seventeen percent of the 128 μm particles have been deposited along the tube wall. While the small particle deposition rate increased by only thirty percent, the large particle deposition rate increased by 165 percnet.

The net effect of the increased interaction coefficient is to increase the combined deposition rate of all of the particles by seventeen percent near the tube entrance and by fifteen percent near the tube exit.

Since no conclusive experimental data exists to verify either form of the interaction coefficient, both forms were considered and serve to provide upper and lower limits for the values of f_i.

A final comparison for the 19 mm x 3.61 m tube may be made by calculating the deposition rate that would occur if 100 percent of the slag entering the tube was deposited on the walls within its 3.66 m length. Assuming a linear decline in the deposition rate, the resulting line would intersect the "Rate of Diameter Decrease" axis at .76, and the L/D_p axis at 192. For most of the tube length, this line gives deposition rates two to four times greater than those shown for the 127 μm wall roughness case, and indicates that all test cases produce results well within this upper limit for particle deposition.

Cases 4 and 5 are also for a 19 mm tube, but with a higher inlet air velocity, lower inlet pressure, longer tube length, and greater inlet to exit temperature gradient. The higher flow velocities result in greater values for ε_f, and consequently higher deposition rates than for the shorter 19 mm tube. The average increase in the deposition rates is fifteen percent for the 253 μm wall roughness tubes, and nine percent for the 127 μm wall roughness tubes. Also, for the longer tube length, the exit deposition rates for the two different wall roughness cases are within 4.5 percent of each other, versus eight percent found for the shorter tube.

The test results for both the 38 mm and 50.8 mm tubes were obtained for 253 μm wall roughness. The deposition rates for both tube sizes are less than those for the 19 mm tubes in the entrance regions of the tubes. However, for axial positions further along the tube, less of the total inlet particle concentration has been deposited than for the 19 mm

tubes, and the larger diameter tubes are able to maintain higher deposition rates. This results from the greater volume to surface ratio of the large diameter tubes, which allows them to continue high deposition rates over greater tube lengths. For axial position expressed in meters rather than tube diameters, the 50.8 mm tube maintains the highest deposition rate beyond 3.5 m, while the 19 mm tube has the lowest rate beyond 2.25 m.

A final indication of particle deposition characteristics is shown in Figure 5, which shows the exit concentration profiles for the 19 mm x 3.66 m tube. Exit profiles for all seven test cases lie within one to five percent of these curves, and all concentration profiles have developed to within five percent of their exit shape within the first twenty diameters of the tube.

The curves in Figure 5 indicate the expected effect of form 2 of the interaction coefficient. The profile for large particles is very flat, with the only appreciable drop in particle concentration occurring within a tenth of a tube radius from the wall. The flat profile indicates the lower response of the larger particles to fluid turbulence.

Fluid turbulence has a much greater effect on smaller particles and a more gradual concentration gradient results from this higher mixing effect, as shown in Figure 5 for the 2 μm particle. The higher mobility of the small particles shown in Figure 5 is also manifested by the higher total deposition rates for small particles as is shown in Figure 6.

Friedlander and Johnstone [4] conducted experiments on the deposition of small (1.57 μm) particles in turbulent pipe flow. The experiments were conducted for tubes lined with either glycerol jelly adhesive or pressure sensitive tape, for which no specific roughness values are available. However, by using the defined experimental flow conditions of Friedlander and Johnstone and varying the value of the tube roughness, the model developed in this thesis may be used to predict the deposition rate of a comparable flow system. Although the absence of tube roughness values prevents a conclusive comparison of the experimental and analytic results, the predicted deposition rates from the model for a reasonable range of roughness values are within ten percent of the experimental results.

V. Conclusions

Based on the seven test cases, several important characteristics of particulate deposition may be predicted:

(1) Wall roughness in a flow passage has a significant effect on deposition rates, with higher wall roughness tubes experiencing higher deposition rates.

(2) Small particles are more greatly effected by fluid turbulence and therefore experience greater movement and produce higher deposition rates than larger particles. Particles smaller then 5 μm respond approximately the same to fluid turbulence and experience equal deposition rates. Because the interaction coefficient is inversely proportional to either the second or fourth power of the particle diameter, the deposition rate declines sharply for particles larger than 10 μm in diameter.

(3) Flow systems operating at lower flow velocities have correspondingly lower values for the eddy diffusivity of momentum and therefore lower deposition rates.

(4) Large diameter tubes produce lower deposition rates near the entrance regions of the tubes, but because of their larger cross-sectional areas, they have a greater volume to surface area ratio and maintain higher deposition rates at axial positions further along the tube than the smaller diameter tubes.

VI. Recommendations

(1) The effects of the interaction coefficient on the deposition rate of particles are significant and an effort should be made to experimentally verify the true form of the relationship for $\varepsilon_p/\varepsilon_f$.

(2) The actual relationship of the turbulent energy versus frequency distribution for low Reynolds number flows is not known and should be investigated to insure realistic values for the particle interaction coefficients.

(3) The results of this work are based on the assumption that no further particle motion occurs after impact with the wall. This is not the actual case for high temperature flow in vertical tubes, and the related problems of particle re-entrainment in the air flow and particle viscous flow down the tube wall should be considered.

TABLES

Table 1: Test Case Particle Size Distribution

Particle Diameter (μm)	Weight %
1.587	1.8
2	2.1
2.52	2.7
3.175	3.7
4	4.6
5.04	5
6.35	5.2
8	5.4
10.1	6.4
12.7	7.1
20.2	7.8
25.4	8.7
32	8.2
40.3	7.1
50.8	6.1
64	5
80.6	3.2
101.6	1.6
128	.8

Obtained from an analysis performed by Coulter Electronics, Co., Hialeah, Florida. Ash sample obtained from the Corette Power Plant, Billings, Montana, and lignite coal from the Rosebud coal seam in Colstrip, Montana.

Table 2: Test Case Flow Conditions

All Cases: Particle Density = 2980 Kg/m^3

Total Inlet Weight Concentration of Particles = 1%

Fluid - Air

Case 1,2,3

V_{inlet} = 61 m/sec

Tube diameter = 19 mm

Tube length = 3.66 m

Pressure = 1.01 x 10^5 Pa

L/D_p	T°K	Re
0	1900	3590
32	1870	3620
66	1830	3660
92	1790	3720
118	1750	3770
158	1670	3870
184	1610	3950

Case 1:

Wall roughness = 127 μm

Case 2:

Wall roughness = 253 μm

Case 3:

Wall roughness = 253 μm

Increased interaction coefficient

Case 4,5

V_{inlet} = 76 m/sec

Tube diameter = 19 mm

Tube length = 6.1 m

Pressure = 9.2 x 10^4 Pa

L/D_p	T°K	Re
0	1900	4050
52	1820	4150
105	1730	4270
157	1610	4470
210	1470	4700
262	1290	5070
315	1110	5540

Case 4:

Wall roughness = 127 μm

Case 5:

Wall roughness = 253 μm

Table 3: Test Case Flow Conditions

All Cases: Particle Density = 2980 Kg/m^3

Total Inlet Weight Concentration of Particles = 1%

Fluid - Air

Case 6

V_{inlet} = 61 m/sec

Tube diameter = 38.1 mm

Tube length = 7.62 m

Pressure = 1.01×10^5 Pa

L/D_p	T°K	Re
0	1900	7190
33	1880	7220
66	1870	7250
92	1840	7300
118	1820	7360
157	1770	7470
197	1730	7590

Wall roughness = 253 μm

Case 7

V_{inlet} = 61 m/sec

Tube diameter = 50.8 mm

Tube length = 12.2 m

Pressure = 1.01×10^5 Pa

L/D_p	T°K	Re
0	1900	9570
34	1880	9610
64	1860	9680
99	1830	9760
133	1790	9900
167	1769	10000
207	1700	10200

Wall roughness = 253 μm

FIGURES

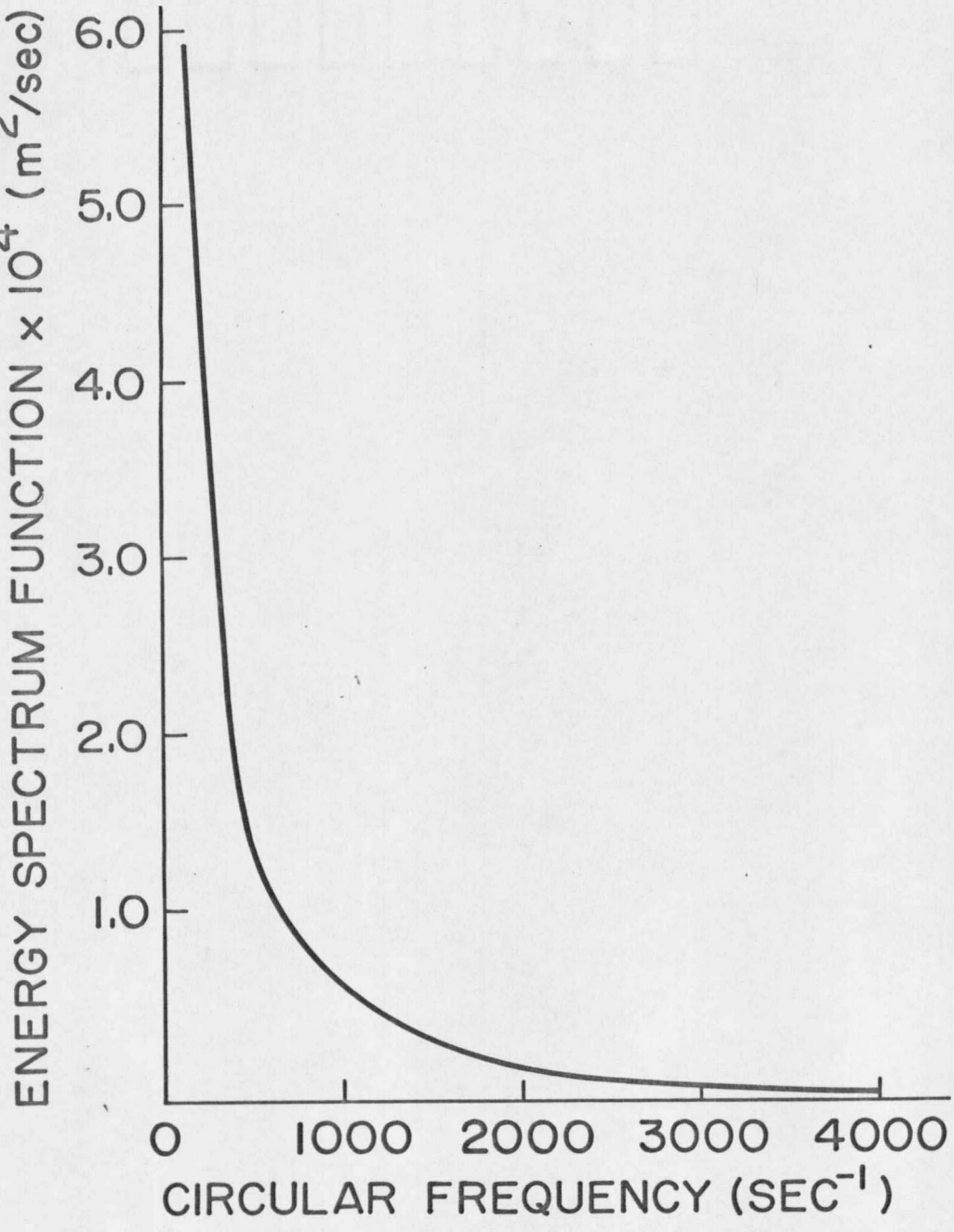


Figure I. Energy Density Spectrum

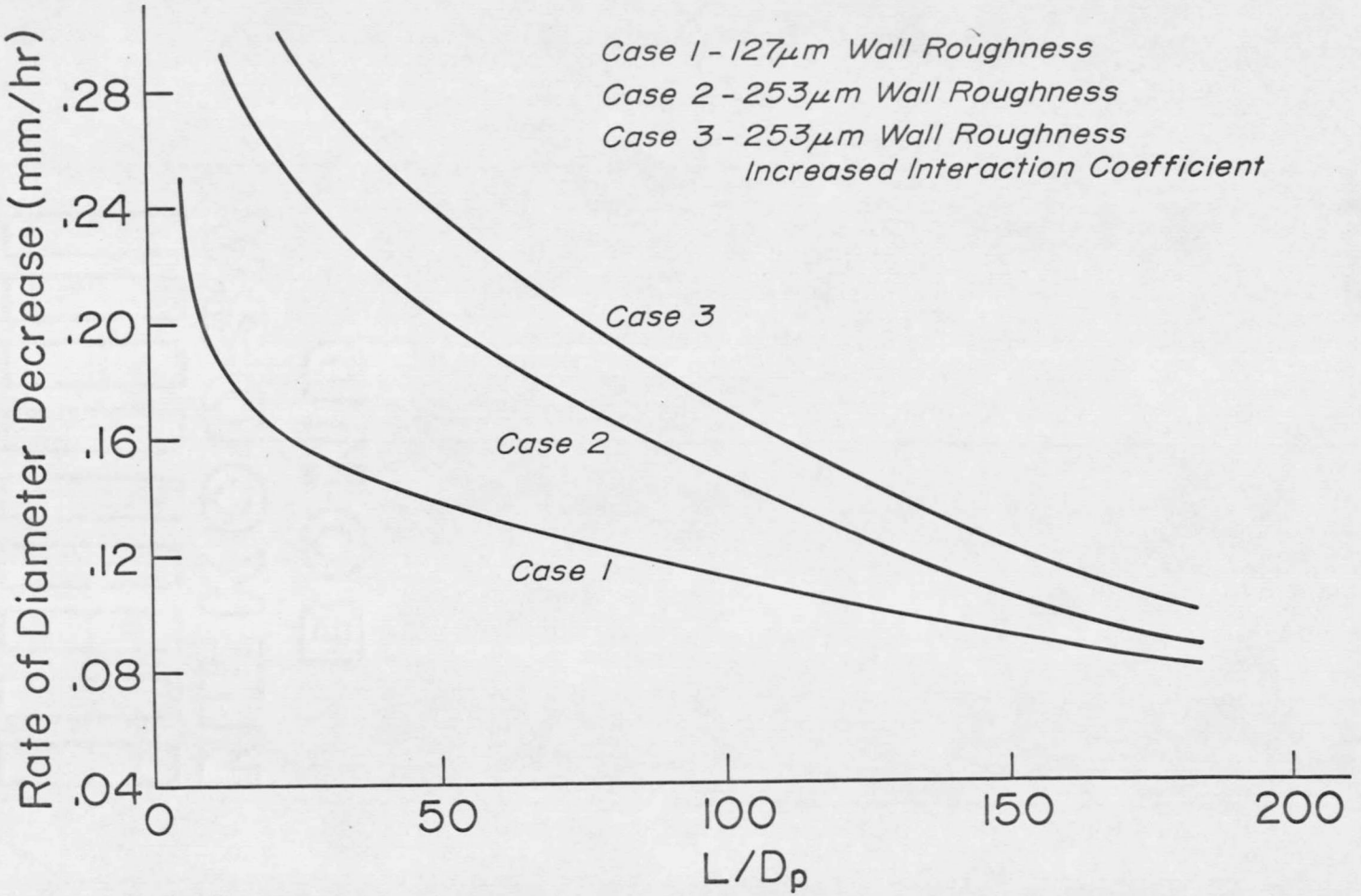


Figure 2. Rate of Diameter Decrease for 19mm x 3.66m Tube

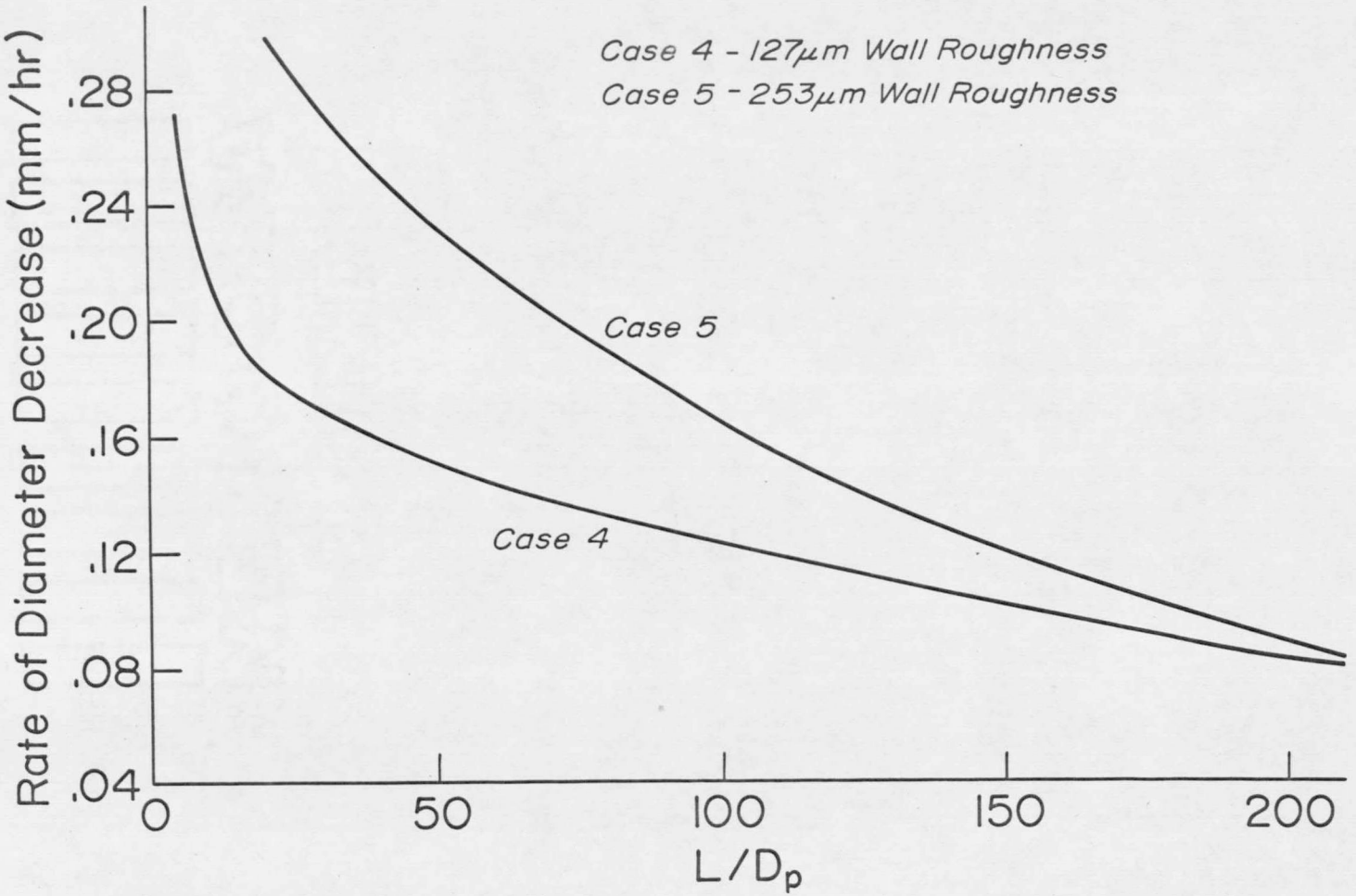


Figure 3. Rate of Diameter Decrease for 19mm x 6.10m Tube

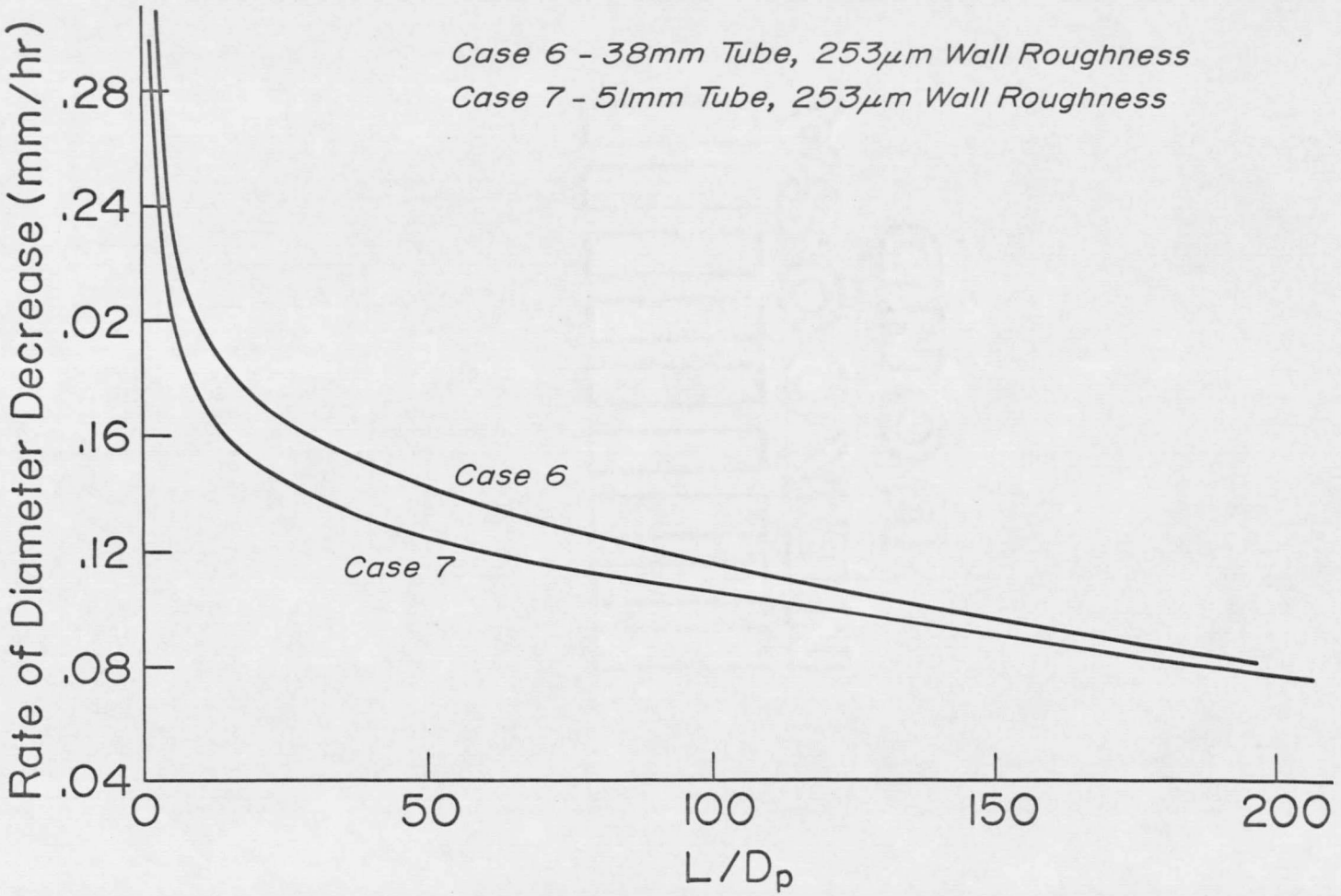


Figure 4. Rate of Diameter Decrease for 38mm x 7.62m and 51mm x 12.2m Tubes

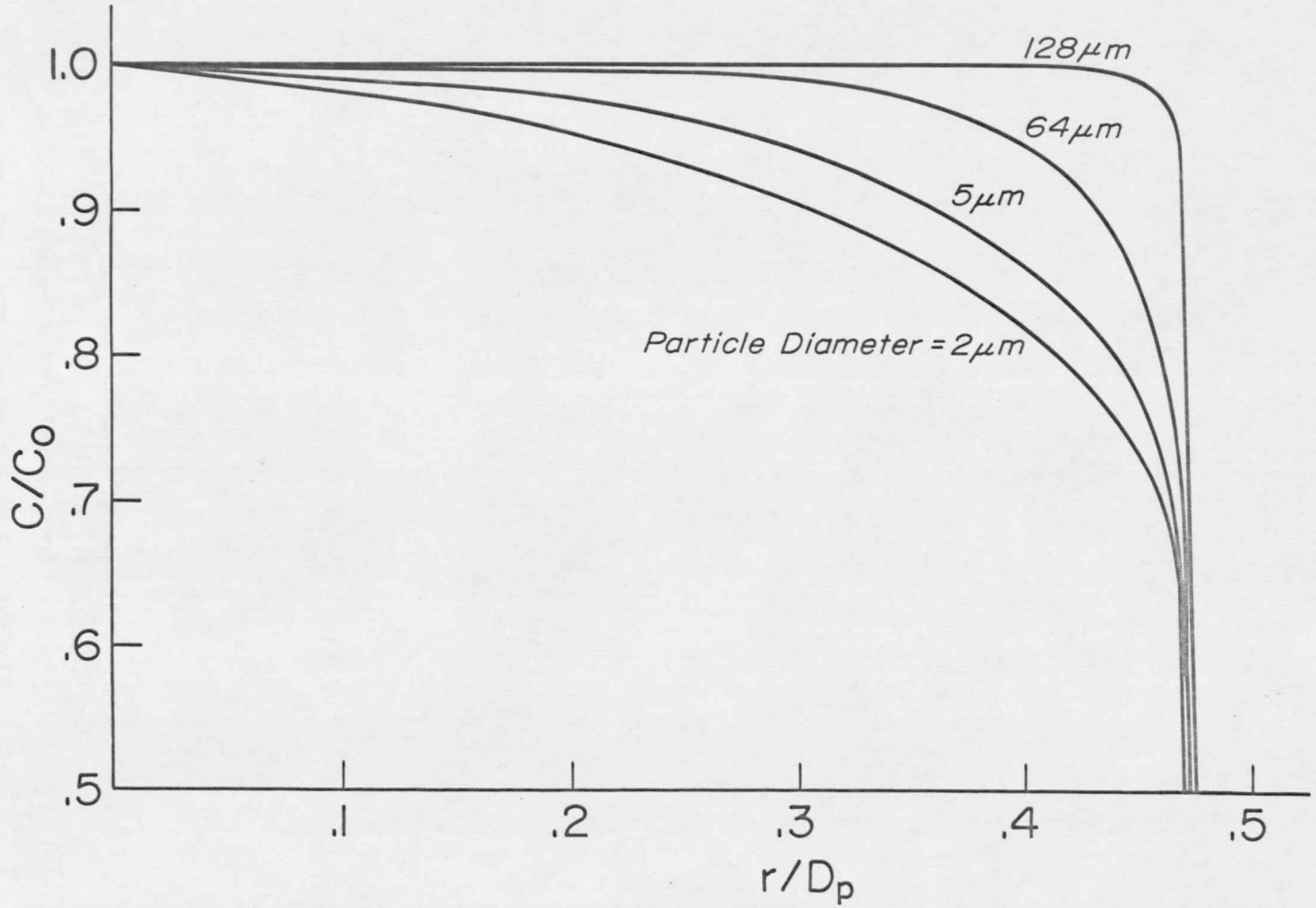


Figure 5. Exit Concentration Profiles for 19mm Tube

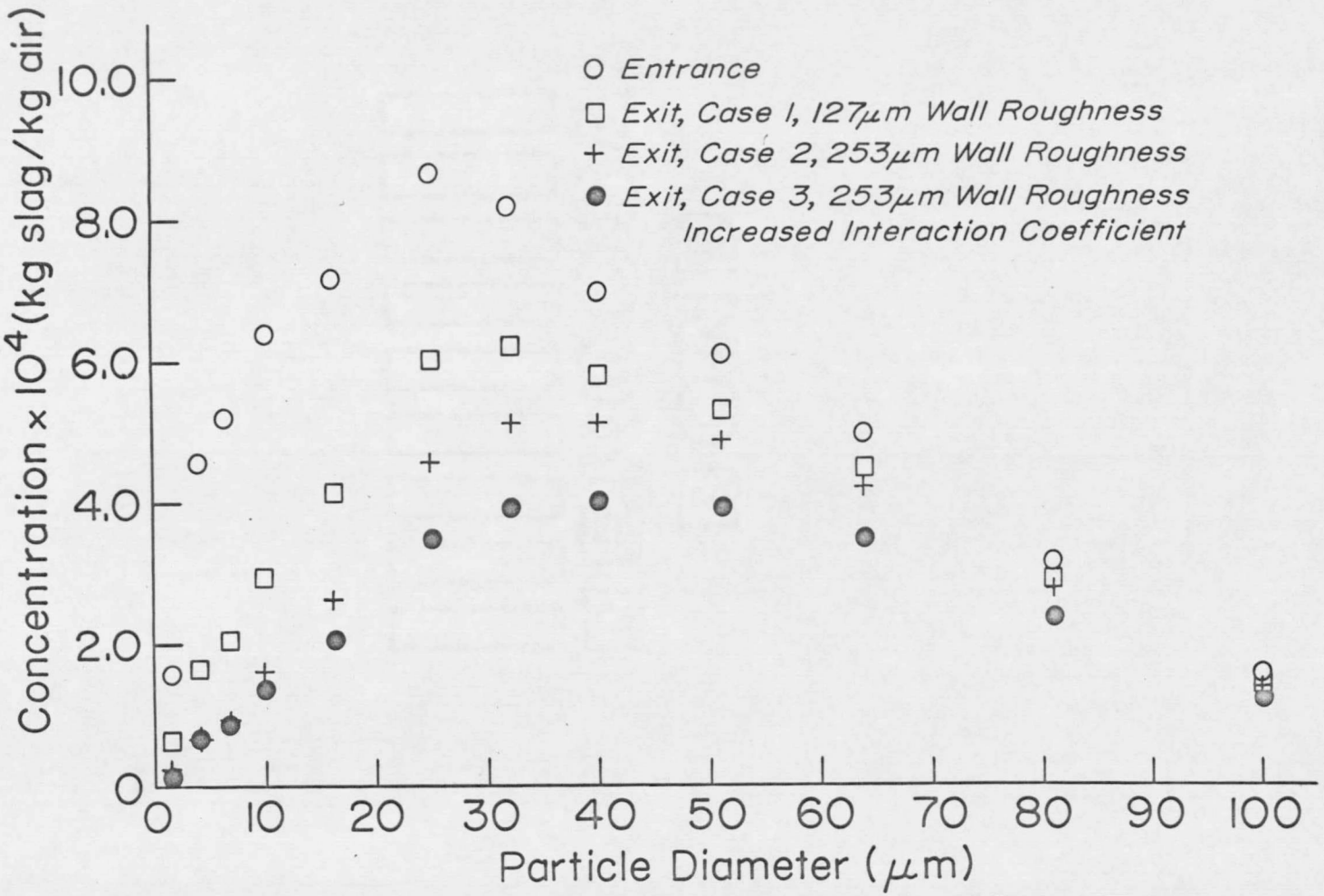


Figure 6. Particle Size Distribution for 19mm Tube

APPENDICES

Appendix I

Development of the equation for turbulent diffusion and bulk transfer of particles in tube flow

The model used to describe the deposition of particulates suspended in a turbulent fluid is based upon a description of the transport of particle mass resulting from molecular and turbulent diffusion due to concentration gradients and bulk transport due to the mean velocity field. The conservation of mass equation in cylindrical coordinates for a cylindrical control volume experiencing both diffusion and bulk transport of mass is [12]

$$\left[\frac{\partial}{\partial r}\left(rD\,\frac{\partial c_v}{\partial r}\right) + \frac{\partial}{\partial z}\left(rD\frac{\partial c_v}{\partial z}\right) + \frac{\partial}{\partial \phi}\left(\frac{D}{r}\,\frac{\partial c_v}{\partial \phi}\right)\right]$$

$$- \left[\frac{\partial}{\partial r}(c_v v r) + \frac{\partial}{\partial z}(c_v u r) + \frac{\partial}{\partial \phi}(c_v w r)\right]$$

$$= \frac{r\partial c_v}{\partial t} \qquad (1\text{-}1)$$

where D = total (molecular plus turbulent) diffusion coefficient
c_v = particle per unit volume of fluid concentration
r = radial position
z = axial position
ϕ = angular position
v = mean radial velocity
u = mean axial velocity
w = mean angular velocity

The terms in the first set of brackets describe the molecular and turbulent diffusion due to a concentration gradient and the terms in the second set of brackets describe the bulk transfer of particles resulting from the mean velocity flow field.

Equation (1-1) may be simplified by the following approximations:

(1) Axial symmetry causes the net angular transfer of mass to be equal to zero.

(2) The mean fluid velocity in the radial direction is zero, and therefore all radial mass transfer is accomplished by diffusion.

(3) The axial diffusion of mass is small relative to the axial bulk transfer of mass so that all particle mass transfer along the tube axis is due to the mean fluid velocity.

(4) The system is at steady flow conditions so that there is no net storage of mass within the tube core.

Based on these four approximations, equation (1-1) may be reduced to

$$\frac{\partial}{\partial r}\left(rD\,\frac{\partial c_v}{\partial r}\right) - \frac{\partial}{\partial z}\left(c_v u r\right) = 0 \qquad (1\text{-}2)$$

At this point, the substitution

$$c_v = c\rho_f \qquad (1\text{-}3)$$

is made, where c is the slag concentration on a mass per unit mass of fluid basis, and ρ_f is the density of the fluid. Substitution of

equation (1-3) into equation (1-2) gives

$$\frac{\partial}{\partial r}\left(rD \frac{\partial}{\partial r}(c\rho_f)\right) - \frac{\partial}{\partial z}\left(uc\rho_f r\right) = 0 \qquad (1\text{-}4)$$

If the equations are used to describe the flow system in the tube before the deposited layer of slag significantly decreases the tube diameter, the tube cross-sectional area is constant and mass flux of fluid, $u\rho_f$, is constant with respect to z. The variable r is also independent of z, and ρ_f is independent of r. Therefore, equation (1-4) may be written as

$$\rho_f \frac{\partial}{\partial r}\left(rD \frac{\partial c}{\partial r}\right) - ru\rho_f \frac{\partial c}{dz} = 0 \qquad (1\text{-}5)$$

Dividing by $ru\rho_f$ and expanding, the resulting equation is

$$\frac{D}{u}\frac{\partial^2 c}{\partial r^2} + \frac{1}{ru}\frac{\partial c}{\partial r}\left(D + r\frac{\partial D}{\partial r}\right) - \frac{\partial c}{\partial z} = 0 \qquad (1\text{-}6)$$

Equation (1-6) is a non-linear partial differential equation, since D is a non-linear function of both r and z. A numerical solution is therefore necessary.

The numerical solution of equation (1-6) poses some problems because of the large gradients in particle concentration, eddy diffusivity, and mean velocity which occur near the tube wall. Because of the large gradients, a relatively small radial step size near the wall

is necessary in the numerical solution, yet these relatively small increments are not required in the core of the tube. A variable radial increment was selected in order to provide the most efficient solution of the problem. The size of the radial increments decreases exponentially from the center of the tube, with the ratio of the increment at the center to the increment at the wall being in the range of 19:1. With the subscripts i and j referring to the radial and axial increments, respectively, the finite difference formulation becomes

$$\frac{\partial c}{\partial z} \rightarrow \frac{c_{i,j+1} - c_{i,j}}{\Delta z} \tag{1-7}$$

$$\frac{\partial c}{\partial r} \rightarrow \frac{c_{i+1,j} - c_{i,j}}{\Delta r_{i+1}} \tag{1-8}$$

$$\frac{\partial^2 c}{\partial r^2} \rightarrow \frac{\dfrac{c_{i+1,j} - c_{i,j}}{\Delta r_{i+1}} - \dfrac{c_{i,j} - c_{i-1,j}}{\Delta r_i}}{\dfrac{\Delta r_{i+1} + \Delta r_i}{2}} \tag{1-9}$$

$$\rightarrow \frac{(\Delta r_i (c_{i+1,j} - c_{i,j}) - \Delta r_{i+1}(c_{i,j} - c_{i-1,j})}{\Delta r_{i+1}\, \Delta r_i \dfrac{\Delta r_{i+1} + \Delta r_i}{2}} \tag{1-10}$$

or

$$\frac{\partial^2 c}{\partial r^2} \rightarrow \frac{\Delta r_i c_{i+1,j} - c_{i,j}(\Delta r_{i+1} + \Delta r_i) + \Delta r_{i+1} c_{i-1,j}}{\Delta r_i\, \Delta r_{i+1} \dfrac{\Delta r_{i+1} + \Delta r_i}{2}} \tag{1-11}$$

where Δz is the axial increment, and Δr_i is the radial increment given by

$$\Delta r_i = r_i - r_{i-1} \tag{1-12}$$

Substitution of equations (1-7) through (1-11) into equation (1-6) gives

$$\frac{D}{u}\left[\frac{\Delta r_i c_{i+1,j} - c_{i,j}(\Delta r_{i+1} + \Delta r_i) + \Delta r_{i+1} c_{i-1,j}}{\Delta r_i \, \Delta r_{i+1} \, \frac{\Delta r_{i+1} + \Delta r_i}{2}}\right]$$

$$+ \frac{1}{ru}\left(D + r\frac{\partial D}{\partial r}\right)\left[\frac{c_{i+1} - c_{i,j}}{\Delta r_{i+1}}\right] \tag{1-13}$$

$$- \frac{c_{i,j+1} - c_{i,j}}{\Delta z} = 0$$

Combining coefficients of like terms and isolating $c_{i,j+1}$ gives

$$c_{i,j+1} = c_{i+1,j}\left[\frac{D}{u}\frac{2\Delta z}{(\Delta r_i + \Delta r_{i+1})}\frac{1}{\Delta r_{i+1}} + \frac{\Delta z}{ru}\frac{1}{\Delta r_{i+1}}\cdot\left(D + r\frac{\partial D}{\partial r}\right)\right]$$

$$+ c_{i,j}\left[-\frac{D}{u}\cdot\frac{2\Delta z}{\Delta r_i \Delta r_{i+1}} - \frac{\Delta z}{ru}\frac{1}{\Delta r_{i+1}}\left(D + r\frac{\partial D}{\partial r}\right) + 1\right]$$

$$+ c_{i,j}\left[\frac{D}{u}\cdot\frac{2\Delta z}{(\Delta r_i + \Delta r_{i+1})}\cdot\frac{1}{\Delta r_i}\right] \tag{1-14}$$

Substitution of the dimensionless parameters

$$\alpha_1 = \frac{\Delta z}{ru\Delta r_{i+1}} \left(D + r \frac{\partial D}{\partial r}\right) \tag{1-15}$$

$$\alpha_2 = \frac{2D\Delta z}{u\Delta r_{i+1}} \cdot \frac{1}{\Delta r_{i+1} + \Delta r_i} \tag{1-16}$$

$$\alpha_3 = \frac{2D\Delta z}{u\Delta r_i \Delta r_{i+1}} \tag{1-17}$$

$$\alpha_4 = \frac{2D\Delta z}{u\Delta r_i} \cdot \frac{1}{\Delta r_{i+1} + \Delta r_i} \tag{1-18}$$

into equation (1-13) gives

$$c_{i,j+1} = c_{i+1,j}(\alpha_1 + \alpha_2) + c_{i,j}(1 - \alpha_1 - \alpha_3) + c_{i-1,j}(\alpha_4) \tag{1-19}$$

Relatively simple boundary conditions may be applied to equation (1-19). Axial symmetry provides for a flat concentration profile at the tube center line, i.e.

$$\frac{\partial c}{\partial r} = 0 \quad \text{at} \quad r = 0 \tag{1-20}$$

This zero slope condition may be approximated by setting

$$c_{o,j} = c_{1,j} \tag{1-21}$$

where $c_{o,j}$ and $c_{1,j}$ are the centerline and first radial grid space concentrations, respectively.

The second radial boundary condition is based on the condition that every particle striking the outermost portions of the wall permanently adheres to the wall. This results in a zero concentration of particles at a distance from the wall equal to the sum of the wall roughness plus one particle radius, i.e.

$$c = 0 \qquad \text{at} \qquad y = d/2 + K \tag{1-22}$$

where y is the distance from the wall, d is the particle diameter, and K is the wall roughness.

The equations are valid for a zero wall roughness, but such a condition results in extremely small axial increments being required to maintain stability in the numerical solution. Because of this fact, and since a zero wall roughness condition is unrealistic, no cases were studied for $K = 0$.

The initial condition for the solution of equation (1-19) may be formed to suit a variety of flow situations. For this analysis, a flat concentration profile was assumed at the tube entrance.

Equation (1-19) may be solved for successive axial steps on a digital computer to describe the particle concentration profiles in both the radial and axial directions. The change in concentration may then be related to the particle deposition rate on the tube wall. (See Appendix IV].

Appendix II

Fluid Eddy Diffusivity of Momentum Derivation

The diffusion of particles suspended in a turbulent fluid results from both molecular diffusion and from the interaction between the particles and turbulent fluid eddies. It is therefore necessary to describe the fluid turbulence, as characterized by the eddy diffusivity of momentum, ε_f. An expression for ε_f based on the mean flow properties of the fluid may be derived from the Navier-Stokes equations.

Molecular diffusion is based on kinetic theory, and is characterized by the molecular diffusion coefficient, D_m. As given by Einstein [9] and Davies [3], the equations for the molecular diffusion coefficient are

$$D_m = \frac{kT_k}{F} \cdot \frac{1}{3\pi\mu d} \qquad (2\text{-}1)$$

where

$$F = 1 + \frac{2 \times 10^4}{Pd} [6.32 + 2.01 \exp (1095\ Pd)] \qquad (2\text{-}2)$$

where k is Boltzman's constant, T_k is the absolute temperature in degrees Kelvin, μ is the dynamic viscosity of the fluid, d is the particle diameter in cm, and P is the absolute pressure in cm Hg.

For the system studied, the maximum value of D_m occurs for the smallest particle size, $d = 1.59 \times 10^{-4}$ cm, and is equal to

3×10^{-7} m^2/sec. In contrast, the values obtained for the turbulent diffusion coefficient range from 10^{-5} m^2/sec at a distance from the wall equal to the wall roughness to 2×10^{-3} m^2/sec in the tube core. Based on these values, D_m is seen to be negligible and only the turbulent diffusion of mass is considered.

As stated, the turbulent diffusion of particles results from turbulent fluid motion. An expression for the fluid eddy diffusivity of momentum based on mean flow properties can be derived from the time-averaged Navier-Stokes equations as is done by Schlichting [7]. The resulting expression is

$$\varepsilon_f = \overline{u'v'}/d\bar{u}/dy \qquad (2\text{-}3)$$

where $\overline{u'v'}$ is the time average of the axial and radial fluctuating velocity components and $d\bar{u}/dy$ is the mean velocity gradient.

Laufer [8] related $\overline{u'v'}$ to the mean velocity field to show that

$$\overline{u'v'} = \nu \frac{d\bar{u}}{dy} + \frac{r}{R} u_*^2 \qquad (2\text{-}4)$$

which can be rewritten by making the coordinate transformation

$$r = R - y, \qquad dr = -dy \qquad (2\text{-}5)$$

as

$$\overline{u'v'} = -\nu \frac{d\bar{u}}{dy} + \frac{R-y}{R} u_*^2 \qquad (2\text{-}6)$$

where ν is the fluid kinematic viscosity, R is the tube radius, and u_* is the friction velocity which is given by

$$u_* = \left(\tau_o / \rho_f\right)^{1/2} \tag{2-7}$$

The wall shear stress, τ_o, is defined in terms of the mean fluid velocity, V, as

$$\tau_o = \frac{f_x}{4} \frac{\rho_f V^2}{2g_c} \tag{2-8}$$

For Reynolds numbers less than 10^5, the Blasius expression for f_x is used as

$$f_x = 0.316/Re^{1/4} \tag{2-9}$$

where

$$Re = VD_p/\nu \tag{2-10}$$

Equations (2-7) and (2-8) may be combined to give

$$u_* = V(f_x/8)^{1/2} \tag{2-11}$$

Equations (2-3) and (2-6) may be combined to give

$$\varepsilon_f = -\nu + \frac{R-y}{R} u_*^2 / \frac{d\bar{u}}{dy} \tag{2-12}$$

An expression for $d\bar{u}/dy$ may be obtained by using the two equation mean velocity profile given by Powe, Townes, and Gow [5] as

$$\bar{u} = u_* c_1 \mathrm{Tanh}(x/c_1) \qquad x \leq x_o \tag{2-13}$$

and

$$\bar{u} = u_*(a_1 \ln(x) + b) \qquad x > x_o \tag{2-14}$$

The constants a_1, b_1, c_1, and x_o are empirically determined constants with values of 2.42, 5.98, 14.68, and 27.75, respectively, and were obtained for Reynolds numbers ranging from 6×10^4 to 3×10^5. The parameter x is defined as

$$x = 3yu_*(2-y/R)/(2\nu(2-4y/R + 2y^2/R^2)) \qquad (2\text{-}15)$$

For the flow conditions used in this study, there is little available information on the development of the velocity profile in the entrance region of the tube. Therefore, a fully developed velocity profile is assumed at the tube entrance. For similar flow systems, the actual entrance effects reduce mass diffusion so the results obtained in this analysis will be conservative, giving larger deposition rates than would be expected in the entrance regions of actual flow systems.

Taking the derivative of equation (2-13) gives

$$\frac{d\bar{u}}{dy} = \frac{d}{dy}(u_* c_1 \mathrm{Tanh}(x/c_1))$$

$$= u_* \mathrm{csech}^2(x/c_1)\frac{d}{dy}(x/c_1)$$

$$= u_* \mathrm{sech}^2(x/c_1)\frac{u_*}{\nu}\frac{9-9y/R}{3-4y/R + 2y^2/R^2} \qquad x \leq x_o \qquad (2\text{-}16)$$

Taking the derivative of equation (2-14) gives

$$\frac{d\bar{u}}{dy} = \frac{d}{dy}(u_* a_1 \ln(x) + b)$$

$$= u_* a_1 \frac{1}{x} \frac{d}{dy}(x)$$

$$= u_* a_1 \frac{1}{x} \frac{u_*}{\nu} \frac{9-9y/R}{3-4y/R + 2y^2/R^2} \qquad x > x_o \qquad (2\text{-}17)$$

Combining equations (2-12), (2-16), and (2-17) gives the expressions for ε_f as

$$\varepsilon_f = -\nu + \frac{\nu}{\operatorname{sech}^2(x/c_1)} \frac{3-4y/R + 2y^2/R^2}{9-9y/R} \qquad x \leq x_o \qquad (2\text{-}18)$$

and

$$\varepsilon_f = -\nu + \frac{\nu}{a_1/x} \frac{3-4y/R + 2y^2/R^2}{9-9y/R} \qquad x > x_o \qquad (2\text{-}19)$$

Because the empirically determined constants, a, b, c, and x_o were obtained from experimental data taken for Reynolds numbers between 6×10^4 and 3×10^5 and the Reynolds numbers used in this study range only as high as 4000, a slight modification is necessary in the application of the eddy diffusivity equations. For lower Reynolds number flows, the ε_f curve goes to zero at an appreciable distance from the tube wall. A shift ranging from .01 R to .03 R in the ε_f curve is therefore required to meet the zero value boundary condition at the tube wall.

The flow conditions for this study involve low Reynolds numbers and rough wall tubes. The combination of these two characteristics creates a system whose behavior as having a hydraulically smooth wall or hydraulically rough wall is indeterminate. Because this region of fluid mechanics is not well understood, no attempt has been made to predict the effect of wall roughness in the expression for ε_f.

The derivation of an expression for ε_f provides a description of the fluid turbulence in the tube which may be related to the turbulent diffusion of particles suspended in the fluid. The analysis is done for a flow system operating at conditions between rough wall and smooth wall flow, and the effect of wall roughness on the eddy diffusivity of momentum is not given.

Appendix III

Derivation of the Particle Interaction Coefficient

The primary mechanism of diffusion of particles suspended in a turbulent fluid results from the interaction between the particles and fluid turbulence. Although the effect of fluid turbulence on momentum transfer in the fluid may be characterized by the eddy diffusivity of momentum, ε_f, a similar relationship for the effect of fluid turbulence on the diffusion of suspended particles is not available. Of primary concern in this section is the development of a reasonable relationship between the diffusion of momentum and the diffusion of suspended particles in turbulent flow.

The interaction of a suspended particle with turbulent fluid eddies is described by Hinze [9] in the form of a non-linear partial differential equation which accounts for viscous resistance forces, pressure gradients around the particle, fluid mass acceleration, and the deviation in the flow pattern from steady state conditions. Because of the large ratio of the particle density to the fluid density, a simplification of the equation is used which considers only the viscous resistance forces according to Stoke's Law, given as

$$F_D = 3\pi\mu d(v_f - v_p) \qquad (3\text{-}1)$$

where F_D is the viscous drag force on the particle, μ is the fluid dynamic

viscosity, d is the particle diameter, and v_p and v_f are the particle and fluid velocities, respectively.

Substitution of equation (3-1) into Newton's second law equation, assuming all other body forces are negligible, results in the simplified form of the equation given by Hinze, i.e.

$$F_D = m_p \frac{d}{dt} v_p = 3\pi\mu d(v_f - v_p) \qquad (3\text{-}2)$$

where m_p is the mass of the particle.

If the velocity fluctuations of a turbulent fluid can be represented by a Fourier transform, a spectrum of sinusoids of varying frequency can be used to describe the fluid turbulence. The fluctuating motion at a single frequency may then be characterized as

$$x_f = X_o \sin\omega t \qquad (3\text{-}3)$$

where x_f is the fluid displacement from its mean position, and X_o and ω are the maximum amplitude and frequency of the turbulent fluid fluctuations, respectively. The velocity of a single frequency component of the fluid fluctuations may be expressed as

$$v_f = \frac{dx_f}{dt} = X_o \omega \cos\omega t \qquad (3\text{-}4)$$

Combining equations (3-2) and (3-4) and re-arranging gives

$$m_p \frac{dv_p}{dt} + 3d\pi\mu v_p = 3d\pi\mu X_o \omega \cos\omega t \qquad (3\text{-}5)$$

The particle velocity, v_p, may be written as

$$v_p = \frac{dx_p}{dt} \tag{3-6}$$

where x_p is the particle displacement from its mean position.

Inserting equation (3-6) and the relationship $m_p = \pi d^3 \rho_p / 6$, where ρ_p equals the particle density, into equation (3-5) gives

$$\frac{d^2x_p}{dt^2} + \frac{18\mu}{\rho_p d^2} \frac{dx_p}{dt} = \frac{18\mu}{\rho_p d^2} X_o \omega \cos\omega t \tag{3-7}$$

Equation (3-7) may be rewritten as

$$\frac{d^2x_p}{dt^2} + \alpha \frac{dx_p}{dt} = \beta \cos\omega t \tag{3-8}$$

where $\alpha = 18\mu/\rho_p d^2$

$$\beta = \alpha\omega X_o$$

Using the initial conditions

$$x_p = x_{po} \text{ and } \frac{dx_p}{dt} = v_{po} \text{ at } t = 0 \tag{3-9}$$

the solution to equation (3-8) is

$$x_p = \left(\frac{\beta}{\omega^2+\alpha^2} - \frac{v_{po}}{\alpha}\right) e^{-\alpha t} + x_{po} + \frac{v_{po}}{\alpha} + \frac{\beta}{\omega^2+\alpha^2}\left(\frac{\alpha}{\omega} \sin\omega t - \cos\omega t\right) \tag{3-10}$$

By differentiating equation (3-10), the maximum value of particle displacement, x_{pm}, may be determined as

$$x_{pm} = X_o\left(\frac{\alpha^2}{\omega^2+\alpha^2}\right)^{1/2} \tag{3-11}$$

Dividing by X_o gives the ratio between x_{pm} and the maximum displacement of the fluid as

$$\frac{x_{pm}}{X_o} = \left(\frac{\alpha^2}{\omega^2+\alpha^2}\right)^{1/2} \tag{3-12}$$

The argument is now made that the eddy diffusion coefficient of a particle is proportional only to the amplitude ratio between the particle and the fluid, and that therefore the ratio $\varepsilon_p/\varepsilon_f$ may be expressed as

$$\frac{\varepsilon_p}{\varepsilon_f} = \frac{x_{pm}}{X_o} = \left(\frac{\alpha^2}{\omega^2+\alpha^2}\right)^{1/2} \tag{3-13}$$

Longwell and Weiss [2] use a similar derivation and obtain the same ratio for x_{pm}/X_o as given in equation (3-12). They state that since the frequency of motion of the particle is the same as that of the fluid, its velocity will be reduced in proportion to its amplitude. Furthermore, they theorize that the eddy diffusion coefficient is proportional to the product of velocity and amplitude, and therefore the ratio of $\varepsilon_p/\varepsilon_f$ must be expressed in the form

$$\frac{\varepsilon_p}{\varepsilon_f} = \left(\frac{x_{pm}}{X_o}\right)^2 = \frac{\alpha^2}{\omega^2+\alpha^2} \qquad (3\text{-}14)$$

Although some experimental data on the deposition of small diameter particles is available [4] it is insufficient to verify the correct form of the $\varepsilon_p/\varepsilon_f$ ratio. Therefore, both forms must be considered.

Turbulent flow is composed of different frequencies, and the interaction coefficient in either form is dependent upon the frequency of the velocity fluctuations. The effect of the frequency spectrum of the turbulent flow on the interaction coefficient is given by modified forms of equations (3-13) and (3-14) as

$$\varepsilon_p = \varepsilon_f \cdot \sum_{k=1}^{11} \left(\frac{\alpha^2}{\omega_k^2+\alpha^2}\right)^{1/2} \cdot f_k = \varepsilon_f \cdot f_{i1} \qquad (3\text{-}15)$$

and

$$\varepsilon_p = \varepsilon_f \sum_{k=1}^{11} \frac{\alpha^2}{\omega_k^2+\alpha^2} \cdot f_k = \varepsilon_f \cdot f_{i2} \qquad (3\text{-}16)$$

The summation term in equations (31) and (32) is one possible method for weighting the effect of each frequency band within the frequency spectrum of the turbulence. For this analysis, the spectrum was arbitrarily divided into eleven frequency bands. The weighting factor f_k, is equal

to the fraction of the total turbulent energy contained within each of the eleven frequency bands.

Energy spectrum data for high Reynolds number flow is available from the work of Powe [6]. There is no known empirical data available for low Reynolds number flows, and consequently the data from Powe was utilized for this analysis. It may be reasonable to assume that although the level of turbulence may change with Re, the relative distribution of the energy with respect to eddy frequency remains essentially the same, although the validity of this assumption is somewhat questionable.

Powe's original data gives turbulent energy as a function of both eddy frequency and radial position. However, because turbulent energy is not a strong function of radius, and there is an uncertainty as to the applicability of high Reynolds number data to this study, and because of the increased computations that would be required otherwise, the radial dependence was removed by using the energy density spectrum averaged over all radii at a given frequency. The resulting curve is shown in Figure 1.

Because α involves the reciprocal of the particle radius squared, form 1 of the interaction coefficient will be inversely proportional to the square of the particle diameter; and form 2 will be inversely proportional to the fourth power of the particle diameter. Therefore, f_i will be much smaller for larger particles than for smaller particles.

By assuming Stoke's flow and Fourier transform representation of fluid turbulence, a relationship between the eddy diffusivity of momentum for fluid and the eddy diffusivity of mass for particles was derived in two possible forms. The resulting expressions rely on high Reynolds number flow data for the energy spectrum of turbulent fluid which is questionable when applied to low Reynolds number flow systems.

Appendix IV

Particle Deposition Rate Derivation

It is necessary to relate the change in the particle concentration profiles at adjacent tube cross-sections to the deposition rate of particles on the wall of the tube. The average particle concentration may be derived from the concentration profiles at any given tube cross-section and used to indicate the axial mass flux of particles at that location. The decrease in mass flux between two adjacent tube cross-sections may be directly related to the mass flux of particles to the wall of the tube.

The net flow of particles across any given axial cross-section is given as

$$M_j = \bar{c}_j u \rho_f A \qquad (4\text{-}1)$$

where $\bar{c}_j$ is the average slag concentration for the cross-section on a mass of particles per unit mass of fluid basis, u is the mean fluid velocity in the axial direction, ρ_f is the fluid density and A is the cross-sectional area of the tube.

The difference in the axial flow of particles at two adjacent tube cross-sections spaced Δz apart equals the net amount of particles deposited on the walls within that Δz section of the tube. This mass flow rate may be changed to a mass flux by dividing by the surface

area of the tube increment between the cross-sections to give

$$\dot{m}_D = (\dot{M}_j - \dot{M}_{j-1})/2\pi R\Delta z \qquad (4\text{-}2)$$

$$= [(\overline{cu}\rho_f A)_j - (\overline{cu}\rho_f A)_{j-1}]/2\pi R\Delta z \qquad (4\text{-}3)$$

Since $u\rho_f A$ is a constant equal to $(u\rho_f)_{inlet} \cdot \pi R^2$, equation (4-3) may be rewritten as

$$\dot{m}_D = (\overline{c}_j - \overline{c}_{j-1})\ (u\rho_f)_{inlet}(R/2\Delta z) \qquad (4\text{-}4)$$

The average particle concentration at any tube cross-section may be determined from the concentration profile. The mass of particles contained within any cross-sectional volume of the tube may be expressed as the sum of the masses contained within several differential elements. The mass contained in the center element of the cross-section is

$$\Delta m_{o,j} = c_{o,j}\Delta\forall_o\rho_f = c_{o,j}\left(\frac{\Delta r_1}{2}\right)^2 \pi\Delta z\rho_f \qquad (4\text{-}5)$$

The mass contained in each of the surrounding annular volumes of the tube cross-section is

$$\Delta m_{i,j} = c_{i,j}\Delta\forall_i\rho_f = c_{i,j}\ \frac{\Delta r_i + \Delta r_{i+1}}{2}\ 2\pi r_i\Delta z\rho_f \qquad (4\text{-}6)$$

Because of the boundary condition of zero particle concentration at the wall, $\Delta m_{i,j}$ at the wall is equal to zero. The total mass contained in any

tube cross-sectional volume is

$$M_j = \sum_{i=0}^{N-1} \Delta m_i = c_{o,j}\left(\frac{\Delta r_i}{2}\right)^2 \pi \Delta z \rho_f + \sum_{i=1}^{N-1} c_{i,j} \frac{\Delta r_i + \Delta r_{i+1}}{2} 2\pi r_i \Delta z \rho_f \quad (4\text{-}7)$$

Another expression for the total mass in a cross-sectional segment of the tube is given by the product of the average particle concentration, $\bar{c}_j$, the fluid density, and the segment volume,

$$M_j = \bar{c}_j \cdot \rho_f \pi R^2 \Delta z \quad (4\text{-}8)$$

Equating equation (4-7) and (4-8) and dividing by $\pi R^2 \Delta z \rho_f$ gives

$$\bar{c}_j = \frac{1}{R^2}\left[c_{o,j}\left(\frac{\Delta r_i}{2}\right)^2 + \sum_{i=1}^{N-1} c_{i,j}(\Delta r_i + \Delta r_{i+1}) r_i\right] \quad (4\text{-}9)$$

Substitution of equation (4-9) into equation (4-4) results in the expression

$$\dot{m}_D = \left[\left[c_{o,j}\left(\frac{\Delta r_i}{2}\right)^2 + \sum_{i=1}^{N-1} c_{i,j}(\Delta r_i + \Delta r_{i+1}) r_i\right] - \left[c_{o,j-1}\left(\frac{\Delta r_i}{2}\right)^2 + \sum_{i=1}^{N-1} c_{i,j-1}(\Delta r_i + \Delta r_{i+1}) r_i\right]\right] \frac{(\rho_f u)_{\text{inlet}}}{2R\Delta z} \quad (4\text{-}10)$$

Equation (4-10) gives the particle deposition rate at any axial position in mass/unit area/unit time. If the slag particles hitting the wall are assumed to permanently adhere to the wall, a layer growth rate may be obtained by dividing $\dot{m}_D$ by the particle density ρ_p,

$$\dot{R} = \dot{m}_D/\rho_p \qquad (4\text{-}11)$$

The layer growth rate would then be equal to the rate of decrease of the tube radius.

By assuming that particles striking the tube wall are permanently held at that point, a relationship between the particle concentration profiles and the particle deposition rate is established.

LITERATURE CITED

LITERATURE CITED

1. Schlinger, W.G. and B.H. Sage, "Material Transfer in Turbulent Gas Streams", Industrial and Engineering Chemistry, Vol. 45, No. 3, March 1953.

2. Longwell, J.P. and M.A. Weiss, "Mixing and Distribution of Liquids in High-Velocity Air Streams", Industrial and Engineering Chemistry, Vol. 45, No. 3, March 1953.

3. Davies, C.N., Aerosol Science, Academic Press, London, New York (1960).

4. Friedlander, S.K. and H.F. Johnstone, "Deposition of Suspended Particles from Turbulent Gas Streams", Industrial and Engineering Chemistry, Vol. 49, No. 7, July 1957.

5. Powe, R.E., Townes, H.W. and J.L. Gow, "Mean Velocity Profiles for Turbulent Shear Flow", Journal of Hydronautics, Vol. 6, No. 1, January 1972.

6. Powe, R.E., "Turbulence Structure in Smooth and Rough Pipe", Doctor of Philosophy Thesis, Mechanical Engineering Dept, Montana State University, December 1970.

7. Schlichting, H., Boundary Layer Theory, McGraw-Hill Book, Co., New York (1960).

8. Laufer, J., "The Structure of Turbulence in Fully Developed Pipe Flow", NACA, TN 1174 (1953).

9. Einstein, A., "Über die von der molekularkinetischen Theorie der Wärme geforderte Bewegung von in ruhenden Flüssigkeiten suspendierten Teilchen", Annal. Physik, No. 17, p. 549 (1905).

10. Hinze, J.O., Turbulence, McGraw-Hill, New York (1975).

11. Eckert, E.R.G. and R.M. Drake, Jr., Heat and Mass Transfer, McGraw-Hill Book, Co., New York (1959).

12. Olson, R.M., Engineering Fluid Mechanics, International Textbook, Co., Scranton, Penn. (1970).

13. Energy Conversion Alternative Study, ECAS, General Electric, Phase 1 Final Report, NASA-CR 134948, Vol. II, Part 3, SRD-76-011.

MONTANA STATE UNIVERSITY LIBRARIES
3 1762 10015419 2

N378
Sa555
cop.2

Sande, Charles K
The deposition of particulates in turbulent pipe flow

DATE	ISSUED TO
OCT 6	L. Burris 221 S. 3rd 6
JUL 21	103 G-C Ag+

N378
Sa555
cop 2